Oceanologia, 68 (4)/2026, 68404
Polish Academy of Sciences
Institute of Oceanology
Open access article under the CC BY license
https://doi.org/10.5697/FTVD6491

Development of a Fuzzy Composite Index for spatial coastal vulnerability assessment under climate change scenarios: A case study of the Makran Coast, Iran

Faeze Chehrazar[1], Esmail Salehi[1,*], Ahmad Nohegar[1], María-José Prados[2], Majid Habibi Nokhandan[3]

Abstract
Coastal zones face increasing pressure from climate change and socioeconomic development, requiring robust, spatially explicit vulnerability assessments. This study develops an integrated Fuzzy Composite Coastal Vulnerability Index (FCVI) to evaluate spatial patterns of vulnerability along the Makran coast (Chabahar–Konarak, Iran) under three climate scenarios (SSP1-2.6, SSP2-4.5, and SSP5-8.5). The framework integrates physical exposure from the InVEST Coastal Vulnerability model (version 3.19.0) with socioeconomic sensitivity and adaptive capacity, standardized using fuzzy logic in a GIS environment. The results reveal pronounced scenario-dependent shifts in both the extent and spatial configuration of vulnerability classes. The area classified as low vulnerability decreases from 1,315,095 ha under SSP1-2.6 to 1,096,947 ha under SSP2-4.5, while high-vulnerability areas increase from 396,095 ha to 498,223 ha. Under the high-emission SSP5-8.5 scenario, high-vulnerability areas expand further to 521,574 ha, accompanied by a marked reduction in moderate-vulnerability areas, from 616,608 ha to 420,038 ha. Beyond these quantitative changes, the results indicate a clear spatial reorganization of vulnerability patterns. Under lower-emission scenarios, high-vulnerability areas remain relatively fragmented and localized, whereas under SSP5-8.5, they become more continuous and spatially connected. This transition suggests a nonlinear response, whereby increasing climatic pressure may induce structural changes in the spatial distribution of vulnerability rather than a simple linear increase. The proposed framework provides a consistent and transferable approach for identifying emerging vulnerability hotspots and supporting scenario-based coastal planning, particularly in data-scarce regions.

Keywords
Coastal vulnerability; Fuzzy Composite Vulnerability Index (FCVI); SSP scenarios (CMIP6); InVEST Coastal Vulnerability; Sea-level rise; Exposure–sensitivity–adaptive capacity; Makran coasts (Chabahar–Konarak)

[1]*Faculty of Environment, University of Tehran, Tehran, Iran*
[2]*Faculty of Human Geography, University of Sevilla, Sevilla, Spain*
[3]*Research Institute of Meteorology and Atmospheric Science (RIMAS), Tehran, Iran*
***Correspondence**: tehranssaleh@ut.ac.ir (E. Salehi)

Received: 3 July 2026; **revised:** 22 September 2026; **accepted**: 15 October 2026

1. Introduction

Coastal zones are among the most dynamic and complex natural systems on Earth, shaped by the continuous interaction of geomorphological processes, geological characteristics, wave dynamics, ocean currents, and tidal regimes. These systems are inherently dynamic and subject to constant change; however, in recent decades, the intensity and rate of their transformation have increased significantly under the growing influence of climate change. Sea-level rise, the intensification and increased frequency of storm events, shifts in precipitation patterns, and ocean warming are among the most critical consequences of climate change, all of which directly affect the stability of coastal environments (IPCC, 2024; Pang et al., 2023). Recent studies have further confirmed the role of climatic variability in amplifying environmental pressures and increasing the occurrence of extreme coastal events (Vousdoukas et al., 2020).

Although coastal areas account for a relatively small proportion of the global land surface, they host a disproportionately large share of the world's population and infrastructure. It is estimated that more than 10% of the global population resides in low-elevation coastal zones (LECZ), with population growth in these areas continuing at a rate exceeding the global average (Reimann et al.,

© 2026 The Author(s). This is the Open Access article distributed under the terms of the Creative Commons Attribution Licence.

2023). Projections indicate that by 2050, the population inhabiting coastal regions will increase substantially (Neumann et al., 2015). This demographic concentration, coupled with rapid infrastructure development and escalating climatic hazards, has significantly increased the likelihood of losses associated with coastal flooding, storms, and erosion, thereby substantially exacerbating the vulnerability of both natural and human systems (Reimann et al., 2023).

Coastal change is not driven solely by climate-related processes; anthropogenic interventions also play a decisive role in altering the morphology and dynamics of these environments. Activities such as beach nourishment, the construction of seawalls, breakwaters, groynes, and port infrastructure significantly modify sediment transport pathways and disrupt natural coastal dynamics. These human-induced alterations, interacting with natural processes such as waves, currents, tides, and coastal storms, generate a highly complex system of feedback interactions (Thieler and Hammar-Klose, 1999; Boumpoulis et al., 2025). The coexistence of these natural and anthropogenic complexities has rendered the assessment of coastal vulnerability a multidimensional and challenging task.

Under such conditions, evaluating coastal vulnerability to climate-induced hazards has gained increasing importance. Risk assessment frameworks are commonly structured around three main components: hazard, exposure, and vulnerability (IPCC, 2014). Vulnerability is a multidimensional concept encompassing sensitivity, adaptive capacity, and the socioeconomic conditions of a system. As emphasized by Füssel and Klein (2006) and Hinkel (2011), a comprehensive vulnerability assessment requires the integration of physical, ecological, and social dimensions within a coherent analytical framework. However, many existing studies have either focused primarily on biophysical indicators or concentrated solely on socioeconomic dimensions, and the simultaneous integration of these components within a unified framework remains challenging (Hinkel and Klein, 2009; IPCC, 2014). Moreover, the selection and combination of indicators are often constrained by data availability and the specific objectives of each study (Arkema et al., 2013; Bevacqua et al., 2018).

In recent years, ecosystem-based approaches, including the InVEST Coastal Vulnerability model, have been increasingly applied to assess coastal exposure and vulnerability across different spatial and temporal contexts. These approaches account for the protective role of natural habitats in reducing exposure to coastal hazards such as storm waves, inundation, and erosion, thereby supporting the assessment of climate-related risks and management alternatives (Arkema et al., 2013; Hopper and Meixler, 2016; Sajjad et al., 2018 The application of such tools has played a significant role in identifying critical coastal zones and enhancing coastal resilience. However, their focus has predominantly remained on biophysical dimensions, while socioeconomic components and future climate scenarios have often been incorporated in a limited or simplified manner.

Alongside these approaches, composite coastal vulnerability indices have been developed to integrate multiple dimensions of vulnerability within a unified framework using multicriteria decision-making techniques (Abijith et al., 2023). Among these, the Fuzzy Composite Coastal Vulnerability Index (FCVI) has emerged as a widely adopted framework due to its ability to handle uncertainty, perform nonlinear normalization of indicators, and simultaneously integrate biophysical and socioeconomic components. As highlighted by Cruz-Ramírez (2024), the FCVI framework has been further expanded in recent studies to incorporate human pressures, development patterns, and social indicators, thereby improving the understanding of coastal hazard dynamics (Sfreddo et al., 2023).

Despite these advancements, existing applications of FCVI still face several limitations. Notably, there is a lack of multi-hazard frameworks capable of simultaneously capturing the combined effects of sea-level rise, storm surges, and coastal erosion (Deb et al., 2019, 2024; Mullick et al., 2024; Zhang et al., 2024). Furthermore, the integrated role of population dynamics, land-use change, and the degradation of ecosystem services has not been sufficiently addressed in many previous studies, particularly in highly dynamic coastal environments such as the Makran coast. These gaps highlight the need for more comprehensive frameworks capable of jointly assessing the multiple dimensions of coastal vulnerability under future climate scenarios (Mafi-Gholami et al., 2019).

2. Material and methods

2.1 Study area

The Makran coastal zone, extending along the northern margin of the Arabian Sea and the Makran subduction system, represents one of the most dynamic and strategically significant coastal regions in southern Iran. This area has been shaped by the combined influence of active tectonic processes, marine dynamics, and warm to semiarid climatic conditions, resulting in a highly complex environmental setting characterized by diverse natural hazards (Motaghi et al., 2020).

The present study focuses on the coastal counties of Chabahar and Konarak in Sistan and Baluchestan Province, which constitute the easternmost coastline of Iran and host the country's only oceanic port (Figure 1). These two counties serve as key hubs for maritime, fisheries, and trade-related activities and play a pivotal role in Iran's coastal development strategy. In recent decades, rapid infrastructure expansion, urban growth, and population increase have significantly altered coastal land-use patterns, particularly in low-lying areas. These transformations have intensified the exposure of settlements, infrastructure, and economic assets to coastal hazards (Pourkerman et al., 2022).

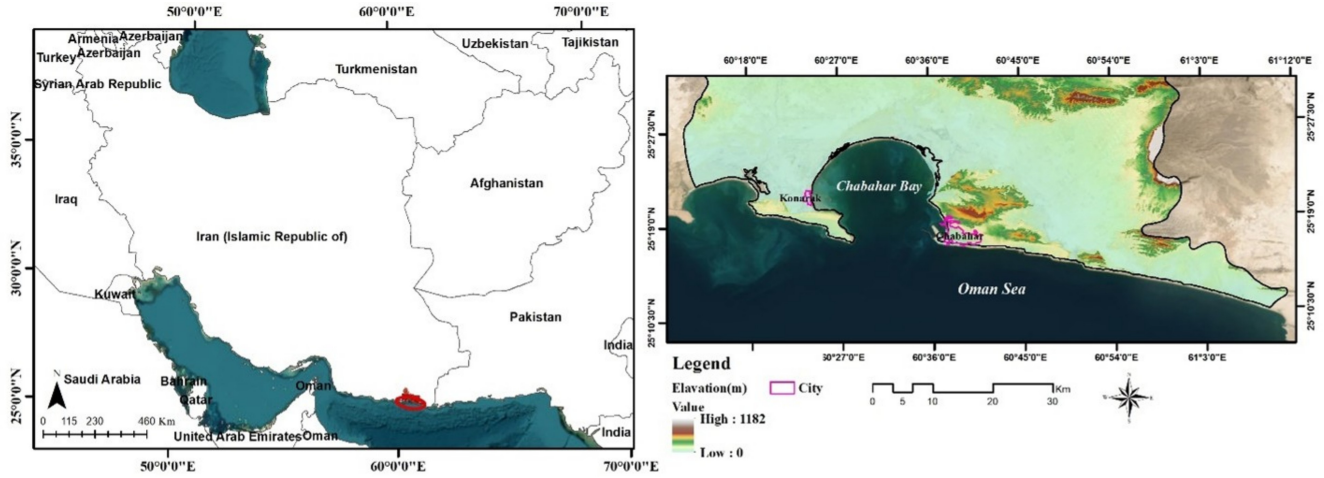


Figure 1. Location map of the study area at regional and local scales.

The regional climate is characterized as hot arid to semiarid coastal, strongly influenced by the Indian Ocean monsoon system. The dominant climatic features include high temperatures, intense evaporation rates, and low but highly concentrated short-duration rainfall events, which frequently lead to flash flooding. In addition, the coasts of Chabahar and Konarak are exposed to a range of marine hazards, including tropical storms, wave surges, severe sea states, and coastal erosion, all of which have increased in both frequency and intensity under the influence of climate change (Mafi-Gholami et al., 2019).

From a geomorphological perspective, the coastline comprises sandy beaches, intertidal flats, estuaries, deltas, rocky headlands, and low-lying coastal plains. These geomorphic units exhibit varying responses to hydrodynamic forces, sea-level fluctuations, and sediment transport dynamics, resulting in spatially heterogeneous levels of coastal sensitivity and vulnerability. The concentration of urban areas, port facilities, and engineered structures within these sensitive geomorphic settings has further amplified overall vulnerability (Ghaderi and Rahbani, 2024).

Given the anticipated population growth and accelerated coastal development, Chabahar and Konarak are expected to face increasing pressure from both climate change and anthropogenic activities. The coexistence of geomorphological diversity, high-energy marine processes, and rising socioeconomic exposure provides a robust framework for comprehensive spatial vulnerability assessment. Such an approach can serve as a scientific basis for integrated coastal zone management and climate change adaptation planning in the region (Motaghi et al., 2021; Pourkerman et al., 2022).

Coastal planning and management in the Makran region are governed by Iran's national legal framework for maritime areas and the institutional arrangements associated with Integrated Coastal Zone Management (ICZM). Under the Law on the Maritime Areas of the Islamic Republic of Iran in the Persian Gulf and the Sea of Oman, the territorial sea extends 12 nautical miles (approximately 22.2 km) from the established baselines, while the contiguous zone extends to 24 nautical miles. The law also establishes Iran's rights and jurisdiction over the Exclusive Economic Zone and continental shelf (Government of the Islamic Republic of Iran, 1993; United Nations, 2026). At the institutional level, the Ports and Maritime Organization (PMO), in coordination with relevant governmental institutions and provincial authorities, plays a central role in the development and refinement of ICZM studies. Iran's national ICZM plan was developed with the participation of 18 institutions, organizations, and ministries and was subsequently approved by the Supreme Council of Urban Planning and Architecture (Ports and Maritime Organization, 2014; Iranian Marine Engineering Association, 2017).

The coastal area examined in the present study is located within this broader coastal and maritime setting governed by Iran's legal and institutional framework. The legally defined maritime zones provide the jurisdictional framework for the governance and management of coastal and marine areas, whereas the spatial extent used in this study represents the analytical area selected for the FCVI assessment. Accordingly, the study area falls within the broader framework of Iran's legally regulated coastal and maritime areas, while the specific spatial extent analyzed in the FCVI was defined according to the requirements of the coastal vulnerability assessment. This distinction clarifies the relationship between the legal framework governing the coastal and maritime areas and the analytical extent used in the present study.

2.2 Conceptual framework for coastal vulnerability assessment

The assessment of coastal vulnerability in this study is based on the widely used three-component framework in climate change research, which conceptualizes vulnerability as the result of the interaction among exposure, sensi-

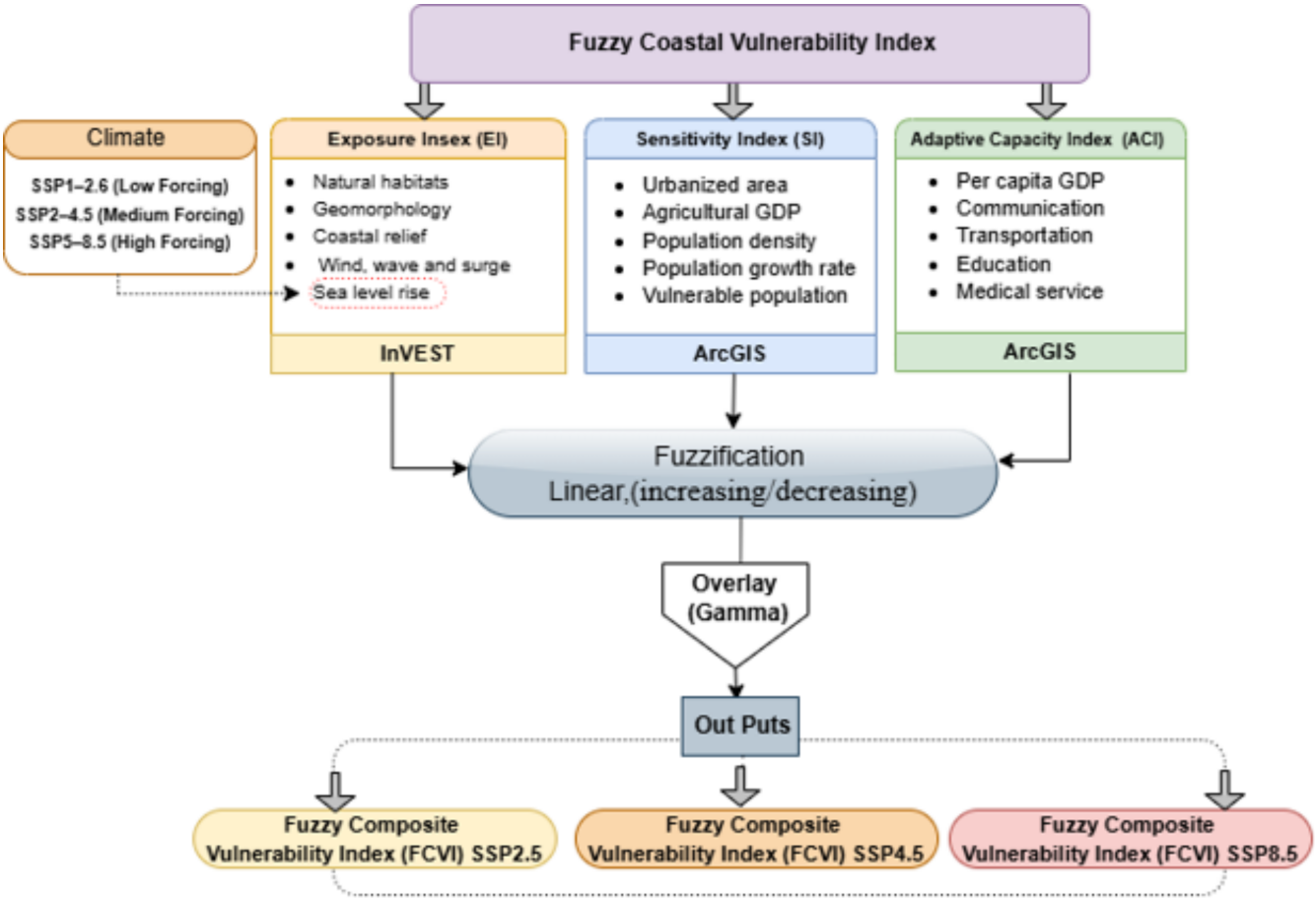


Figure 2. Conceptual flowchart of the Fuzzy Composite Coastal Vulnerability Index (FCVI) calculation process.

tivity, and adaptive capacity. Within this framework, exposure refers to the degree to which the coastal system is subjected to physical hazards driven by marine processes and climate change impacts. Sensitivity represents the extent to which human and environmental elements are affected by these hazards, while adaptive capacity reflects the ability of the system to cope with, adjust to, and mitigate the adverse effects of changing conditions. The integration of these three components enables a comprehensive spatial analysis of vulnerability and has been extensively applied in climate risk assessment and adaptation planning studies.

In this research, building upon this conceptual framework, a composite coastal vulnerability index was developed by integrating the aforementioned three components. The Exposure Index (EI) was derived using the Coastal Vulnerability module of the InVEST model, while the Sensitivity Index (SI) and Adaptive Capacity Index (ACI) were constructed from their respective spatial sub-indicators in ArcGIS. Prior to integration, the input layers were standardized using linear fuzzy membership functions, with increasing or decreasing membership relationships selected according to the expected effect of each variable on coastal vulnerability. The standardized EI, SI, and ACI layers were subsequently integrated using the Fuzzy Gamma operator ($\gamma = 0.5$) to generate the final FCVI maps under the SSP1-2.6, SSP2-4.5, and SSP5-8.5 scenarios. The fuzzy membership functions and parameter values used for the input variables are provided in the corresponding tables.

The overall analytical workflow used to construct the Fuzzy Composite Coastal Vulnerability Index (FCVI) is presented in Figure 2. The workflow explicitly follows the sequence of EI, SI, and ACI derivation, fuzzy standardization, and Fuzzy Gamma integration, providing a transparent and reproducible framework for generating the scenario-specific FCVI maps.

2.3 Data and preprocessing

In this study, a comprehensive set of biophysical, socioeconomic, and infrastructural datasets was employed to assess coastal vulnerability based on three components: exposure, sensitivity, and adaptive capacity (Table 1). The datasets required for modeling coastal exposure included physical and hydrodynamic variables related to coastal conditions and marine processes, which were used as inputs to the Coastal Vulnerability model in InVEST (Arkema et al., 2013; Natural Capital Alliance, Stanford University, 2026). In addition, to derive the sensitivity and adaptive capacity

indicators, data related to population characteristics, land use, infrastructure, and other socioeconomic attributes of the study area were collected and transformed into spatial layers.

To ensure data integration within the GIS environment, all layers were harmonized in terms of coordinate reference system, spatial scale, and study extent. Vector datasets were converted into raster format, and all layers were resampled to a consistent spatial resolution to enable spatial analysis and multilayer integration. Furthermore, quality control procedures were conducted, including the removal of incomplete records, correction of spatial inconsistencies, and verification of layer overlaps. These preprocessing steps provided the necessary foundation for implementing the InVEST model, applying fuzzy standardization, and performing subsequent spatial analyses.

2.4 Definition of climate scenarios

To examine the influence of climatic uncertainties on coastal vulnerability, the analyses were conducted under three climate change scenarios based on the Shared Socioeconomic Pathways (SSPs) framework. These scenarios included SSP1-2.6 as a low-emission optimistic scenario, SSP2-4.5 as an intermediate stabilization scenario, and SSP5-8.5 as a high-emission pessimistic scenario. The selection of these three scenarios was intended to capture a broad range of plausible future climatic conditions and to enable comparative assessment of the coastal system's response under varying levels of climate change intensity.

Climate-related variables associated with coastal hazards, particularly those influencing sea-level rise and hydrodynamic conditions, were extracted according to these scenarios and used as inputs to the Coastal Vulnerability module of the InVEST model. Accordingly, a distinct climatic condition set was defined for each scenario, resulting in the generation of separate coastal exposure maps. These outputs formed the basis for subsequent scenario-based vulnerability analysis.

2.5 Exposure Index based on the InVEST model

The Exposure Index (EI) was calculated using the coastal vulnerability assessment framework implemented in the Integrated Valuation of Ecosystem Services and Tradeoffs (InVEST) model, developed by the Natural Capital Project (Arkema et al., 2013; Sharp et al., 2020). This model integrates biophysical hazard drivers with the protective role of coastal ecosystems, enabling a comprehensive assessment of physical exposure and aligning with contemporary frameworks for climate risk and multi-hazard analysis (Oppenheimer et al., 2019; IPCC, 2022).

Given that sea-level rise is one of the most critical drivers of coastal hazard intensification in the 21st century, future sea-level scenarios derived from the Shared Socioeconomic Pathways (SSPs) within the CMIP6 framework were incorporated into the analysis. Specifically, SSP1-2.6, SSP2-4.5, and SSP5-8.5 were selected to represent low, intermediate, and high emission trajectories, respectively (IPCC, 2022). These scenarios correspond to different radiative forcing levels by the end of the century and constitute the main basis for climate projections in the Sixth Assessment Report of the IPCC.

Accordingly, projected sea-level rise values under each scenario were integrated into the coastal vulnerability model, and the relative coastal elevation component was

Table 1. ndicator-based framework for coastal vulnerability assessment

Dimension	Indicator	Reference
Exposure	• Geomorphology • Natural habitats • Coastal relief • Sea-level rise • Wind, wave, and storm surge	Gornitz (1991), Thieler and Hammar-Klose (1999), Arun Kumar and Kunte (2012), Thieler and Hammar-Klose (1999), ElKotby et al. (2024b) Torresan et al. (2020), Hossain et al. (2022) , Oloyede et al. (2022)
Sensitivity	• Urbanized area • Agricultural GDP • Population density • Population growth rate • Vulnerable population	Cutter et al. (2003), Mavromatidi et al. (2018), Oloyede et al. (2022), Le Cozannet et al. (2013), Hossain et al. (2022), Nguyen et al. (2016), Dasgupta et al. (2009), Akash et al. (2024)
Adaptive Capacity	• Per capita GDP • Communication • Transportation • Education • Medical services	Tahri et al. (2017), Akash et al. (2024), Mani Murali et al. (2018), Oloyede et al. (2022)

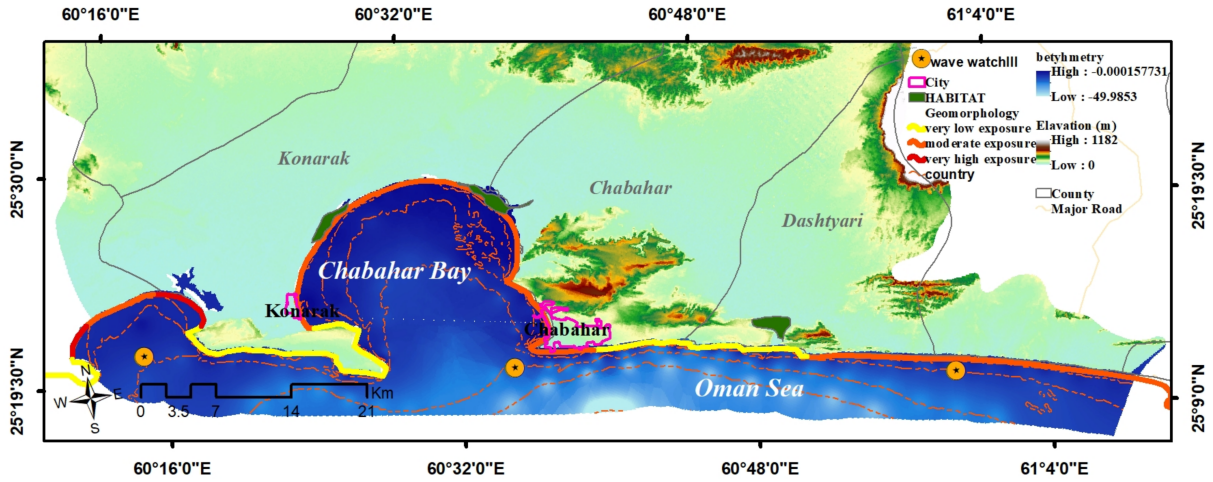


Figure 3. Spatial distribution of the main factors influencing coastal exposure along the Chabahar Bay and Oman Sea coastline.

updated. Other biophysical drivers, including geomorphology, habitat characteristics, and wave dynamics, were assumed to remain constant. The Exposure Index was recalculated for each scenario to evaluate the progressive influence of sea-level rise on hazard intensity along different coastal segments. Recent studies have demonstrated that sea-level rise, when interacting with wave dynamics and storm-induced surges, can synergistically amplify coastal flooding risks (Bevacqua et al., 2020; Mentaschi et al., 2020; Vousdoukas et al., 2020). Accordingly, exposure in this study is defined as the cumulative effect of physical forces acting on each coastal segment, consistent with the emerging understanding of compound climate hazards (Hinkel, 2011; IPCC, 2022).

All exposure-related variables were standardized prior to aggregation and classified into a five-level ordinal scale (1 = very low exposure to 5 = very high exposure), following established approaches in coastal vulnerability studies (Arkema et al., 2013; Krishnan et al., 2019). The Exposure Index for each spatial unit was computed using a geometric mean formulation.

In this study, the exposure component was derived using the Coastal Vulnerability module of the InVEST software. This process-based model integrates key biophysical coastal parameters to spatially assess exposure to climate-related and marine hazards. In the version applied here, the Exposure Index was calculated based on a combination of coastal geomorphology, coastal slope and elevation (DEM), bathymetry, wave climate, storm surge levels, and the protective function of coastal ecosystems. The model output provides a relative exposure index along the coastline, representing the degree to which each coastal segment is subject to physical hazards. Due to its capability to simultaneously incorporate physical processes and ecosystem-based protection services, InVEST has been widely used in coastal vulnerability and risk assessments and was adopted in this study as the basis for estimating the Exposure Index (EI) within the FCVI framework (Figure 3).

To quantitatively assess coastal exposure, a threshold-based index framework was developed in which offshore and local conditions are explicitly considered in a disaggregated manner. In this context, the conditional exposure component is defined as follows:

$$E^k = \sum_{n=1}^{16} I(x_n)\, A_n^k\, B_n^k\, k \in \{o, l\} \tag{1}$$

where k denotes the type of condition, including offshore (o) and local (l) conditions. In this formulation, x_n represents a threshold-dependent variable (such as water depth, fetch conditions, or other hydrodynamic parameters), and h is the critical threshold value defined for activating each component. The indicator function $I(x_n)$ is defined as follows:

$$I(x_n) = \begin{cases} 0 & x_n < h, \\ 1 & x_n \geq h \end{cases} \tag{2}$$

Accordingly, only those parameters that exceed the predefined threshold contribute to the computation of total exposure. The coefficients represent, respectively, the relative weight (or importance) of each factor and the magnitude of its effect under offshore or local conditions. This formulation enables the incorporation of nonlinear behavior and the activation of critical thresholds within the model framework.

To account for environmental energy effects, an energy/potential component was also defined as follows:

$$\phi = 1/2\, \rho^2 \tag{3}$$

where (ρ) is a characteristic parameter representing the intensity or density of hydrodynamic energy acting on the coast. This component serves as a moderating factor that regulates the magnitude of forces exerted on the coastal system.

Finally, the overall coastal exposure is expressed as a function of the hydrodynamic indicators and the conditional components defined above:

$$Exposure = f(REI, E_w, E^o, E^l, \varphi) \quad (4)$$

where REI denotes the Relative Exposure Index, (E_w) represents wave energy, and (E^o) and (E^l) correspond to offshore and local exposure components, respectively. Within this framework, the dominant wave forcing is governed by the maximum contribution of offshore and local conditions, allowing the model structure to capture and integrate hydrodynamic effects across multiple spatial scales.

To investigate the impact of climate change, the model was independently run for each defined climate scenario. Consequently, three separate coastal exposure maps were generated, each representing the degree of coastal hazard exposure under different climatic conditions. The resulting outputs were subsequently exported to the GIS environment for further analysis and served as the basis for fuzzy standardization and integration with other vulnerability components.

The use of the geometric mean was adopted to preserve the noncompensatory nature of the index and to reflect the multiplicative interaction among hazard drivers. In linear additive approaches, high values of one variable can offset low values of others, potentially leading to an underestimation of the actual level of risk (Hinkel, 2011; Tonmoy et al., 2014). In contrast, this formulation prevents such compensation effects and provides a more realistic representation of compound hazard interactions. This structure is consistent with recent recommendations for integrating multihazard risks within climate risk assessment frameworks (Ward et al., 2020; Reimann et al., 2021; IPCC, 2022).

2.6 Sensitivity Index

The Sensitivity Index (SI) was developed to quantify the potential susceptibility of socioeconomic structures to coastal hazards. Within contemporary vulnerability assessment frameworks, sensitivity is defined as an intrinsic characteristic of society, encompassing demographic structure, economic conditions, and social attributes that determine the degree of impact experienced during hazard events (Cutter, 2024).

Based on recent systematic reviews in the field of social vulnerability indicators, variables such as population density, age structure, income level, employment status, and land-use patterns are among the most commonly employed components for sensitivity assessment (Mah et al., 2023; Kim et al., 2025). Accordingly, in the present study, the Sensitivity Index was constructed using a set of demographic and economic sub-indicators, including population density, population growth rate, proportion of urban land, economic dependence on climate-sensitive activities, and the proportion of vulnerable population groups. The sub-indicators used are presented in Table 1. To integrate variables related to vulnerable population groups and reduce internal multicollinearity, Principal Component Analysis (PCA) was applied to derive a composite score.

At the initial stage, 10 socioeconomic variables were examined, including urbanized area, agricultural gross domestic product (GDP), population density, population growth rate, population under 15 years of age, population over 65 years of age, proportion of females, unemployment rate, low-income population, and agricultural employment. To reduce multicollinearity and information redundancy among the variables, PCA was performed on standardized data using Z-scores and the correlation matrix. Components with eigenvalues greater than 1 were retained. Subsequently, representative variables were selected based on their factor loadings and conceptual relevance to socioeconomic sensitivity. Accordingly, five indicators, namely urbanized area, agricultural GDP, population density, population growth rate, and vulnerable population, were retained as the final indicators for calculating the Sensitivity Index (SI). All sub-indicators were standardized prior to aggregation and classified into a five-level ordinal scale (1 = very low sensitivity to 5 = very high sensitivity).

2.7 Adaptive Capacity Index

The Adaptive Capacity Index (ACI) was developed to assess the ability of socioeconomic systems to mitigate the adverse effects of coastal hazards and to adapt to climate change conditions. Within contemporary climate risk assessment frameworks, adaptive capacity refers to the ability of a society to anticipate, cope with, respond to, and recover from hazard events, thereby playing a mitigating role in shaping overall vulnerability (IPCC, 2022).

Recent reviews indicate that adaptive capacity in coastal social-ecological systems is inherently multidimensional and influenced by economic, institutional, educational, infrastructural, and resource-access-related factors (Espinoza Córdova et al., 2024; Serdeczny et al., 2024). These studies emphasize that index-based assessments of adaptive capacity should incorporate not only economic capital but also governance quality, livelihood diversification, human capital, and access to public services (Zhai and Lee, 2024).

Accordingly, in the present study, the Adaptive Capacity Index was constructed based on a set of socioeconomic sub-indicators, including education level, per capita income, access to basic infrastructure, housing quality, economic diversification, and availability of public services. These variables reflect the potential of communities to reduce damages, manage crises, and recover following coastal

hazard events. The sub-indicators used are presented in Table 1.

All sub-indicators were standardized prior to aggregation and classified into a five-level ordinal scale (1 = very low adaptive capacity, 5 = very high adaptive capacity). To preserve the noncompensatory nature of the index and to avoid overestimation of adaptive capacity in cases where only a subset of components performs well, the Adaptive Capacity Index for each spatial unit was calculated using the geometric mean

$$ACI = \left(\prod_{i=1}^{n} R_i \right)^{\frac{1}{n}} \tag{5}$$

where (R_i) denotes the rank of the (i) sub-indicator and (n) represents the total number of adaptive capacity sub-indicators. This approach enables the representation of the interactive effects among different components of adaptive capacity and is consistent with recent recommendations for index-based assessment of social-ecological systems (Espinoza Córdova et al., 2024).

2.8 Fuzzy standardization of indicators

To account for inherent uncertainties in socio-environmental datasets and to represent the gradual nature of changes in vulnerability intensity, the Exposure Index (EI), Sensitivity Index (SI), and Adaptive Capacity Index (ACI) were standardized and integrated using a fuzzy logic approach. Compared with discrete classification methods, fuzzy logic enables the modeling of continuous transitions between different levels of vulnerability and is therefore more suitable for analyzing complex socio-ecological systems.

Recent applications of fuzzy logic in flood-induced social vulnerability assessment have demonstrated that fuzzy membership functions can better capture gradual variations in exposure intensity and avoid artificial boundaries between classes (Moragues et al., 2025). Moreover, the integration of multicriteria decision-making techniques with fuzzy logic in climate risk analysis provides a flexible framework for combining both natural and social drivers of risk (Hodasová et al., 2025). Recent studies in urban flood risk assessment have also shown that coupling geospatial data with fuzzy inference systems improves the spatial accuracy of vulnerability estimation (Muthu and Ramamoorthy, 2025).

In this study, after the initial computation of EI, SI, and ACI using the geometric mean, each index was transformed into a fuzzy membership range of $[0, 1]$. A value of zero represents the lowest degree of membership in the "high vulnerability" set, whereas a value of one indicates the highest degree of membership. Based on the nature of the indicators, an increasing membership function was applied to EI and SI, whereas a decreasing membership function was used for ACI.

For each indicator, the parameters of the linear fuzzy membership function were defined using the lower and upper bounds of the corresponding input layer. The lower threshold represents the value assigned a fuzzy membership of 0, whereas the upper threshold represents the value assigned a fuzzy membership of 1. For indicators positively related to vulnerability, membership values increase linearly from 0 to 1 between the lower and upper thresholds. For indicators negatively related to vulnerability, membership values decrease linearly from 1 to 0 over the same range. The lower and upper thresholds were determined separately for each indicator based on its spatial data range, and the same parameters were applied consistently across the study area and the corresponding climate scenarios.

Fuzzy standardization was carried out as follows:

For increasing indicators (EI and SI):

$$\mu(x) = \begin{cases} 0 & \text{if } x \le a \\ \frac{x-a}{b-a} & \text{if } a < x < b \\ 1 & \text{if } x \ge b \end{cases} \tag{6}$$

For the decreasing indicator (ACI):

$$\mu(x) = \begin{cases} 1 & \text{if } x \le a \\ \frac{b-x}{b-a} & \text{if } a < x < b \\ 0 & \text{if } x \ge b \end{cases} \tag{7}$$

- x = crisp input value
- a = lower threshold
- b = upper threshold

2.9 Scenario-based integration of indicators and generation of final coastal vulnerability maps

After calculating the three main components of vulnerability, including the Exposure Index (EI), Sensitivity Index (SI), and Adaptive Capacity Index (ACI), all outputs were transformed into fuzzy membership values within the [0–1] range to ensure a common scale for integration. Accordingly, for each climate scenario, a fuzzy exposure map was generated, while fuzzy maps of sensitivity and adaptive capacity were independently produced.

In the next step, the fuzzy vulnerability index was computed using the Fuzzy Gamma Operator to preserve the noncompensatory structure of the integration while accounting for both synergistic and interactive effects among the different components. The general formulation of this operator is expressed as follows:

$$\mu_\gamma = (\mu_{sum})^\gamma \times (\mu_{product})^{(1-\gamma)} \tag{8}$$

$$CVI_{\gamma=0.5} = [1-(1-\mu_{EI})(1-\mu_{SI})\mu_{ACI}]^{0.5} \times [\mu_{EI}\,\mu_{SI}\,(1-\mu_{ACI})]^{0.5} \tag{9}$$

This formulation enables the simultaneous representation of uncertainty, nonlinear relationships, and interdependencies among risk drivers and is consistent with recent advances in fuzzy logic–based approaches for multi-hazard vulnerability assessment (Hodasová et al., 2025; Moragues et al., 2025).

To compute the final coastal vulnerability index, the integration process was conducted in a scenario-based manner. Accordingly, for each climate scenario, the corresponding exposure map, together with the sensitivity and adaptive capacity layers, was overlaid using fuzzy combination operators within a GIS environment. This procedure was repeated three times, resulting in a distinct coastal vulnerability map for each scenario. The resulting maps represent the spatial pattern of relative coastal vulnerability under different climatic conditions and enable a comparative analysis of changes in vulnerability across scenarios.

3. Validation method

To assess the spatial consistency of the coastal vulnerability assessment, a total of 20,000 sampling points were systematically extracted along the Makran coastline using Google Earth Pro. The number of sampling points was selected to provide broad spatial coverage of the study area and account for its geomorphological complexity and spatial heterogeneity. Elevation values were extracted for each sampling point from Google Earth Pro and classified into three elevation classes: ≤ 0 m, 0–1 m, and 1–5 m. Sampling points with elevations greater than 5 m were excluded from the elevation-based assessment because the analysis focused on low-lying coastal areas that are more directly relevant to coastal vulnerability. Coastal elevation relative to sea level is a key factor controlling exposure to sea-level rise and coastal flooding, particularly in low-lying coastal environments (Gesch, 2018; Hooijer and Vernimmen, 2021).

The sampling points were subsequently overlaid with the coastal vulnerability maps developed for the SSP1-2.6, SSP2-4.5, and SSP5-8.5 climate change scenarios. For each elevation class and climate change scenario, the number of sampling points falling within the High and Very High vulnerability classes was determined, and the corresponding percentage was calculated using Equation (1):

$$P = (Nv/Nt) \times 100 \tag{10}$$

where (P) represents the percentage of sampling points classified as High or Very High vulnerability, (N_v) represents the number of sampling points falling within the High and Very High vulnerability classes, and (N_t) represents the total number of sampling points within the corresponding elevation class.

The resulting percentages were compared among the three elevation classes for each climate change scenario and subsequently examined across the SSP1-2.6, SSP2-4.5, and SSP5-8.5 scenarios. This comparison was intended to determine whether the modeled vulnerability patterns exhibited a systematic relationship with coastal elevation. In particular, a relatively greater proportion of High and Very High vulnerability points within the lower elevation classes was considered consistent with the expected spatial behavior of coastal vulnerability, because low-lying coastal areas are generally more exposed to elevated coastal water levels, sea-level rise, and coastal flooding (Gesch, 2018; Hooijer and Vernimmen, 2021). Thus, the elevation-based comparison provided a spatial consistency check to determine whether areas identified by the FCVI as having greater vulnerability were preferentially concentrated within coastal settings characterized by lower elevations.

To further examine the spatial coherence of the vulnerability patterns, the distribution of areas classified as High and Very High vulnerability was also evaluated in relation to major geomorphological and hydrological features of the Makran coast. Particular attention was given to river mouths, low-lying coastal plains, and estuarine environments, as these settings may represent areas where the interaction between coastal processes, hydrological conditions, and low terrain elevation can increase exposure to coastal hazards. The spatial correspondence between high-vulnerability areas and these coastal features was therefore examined as an additional qualitative component of the spatial consistency assessment.

Overall, the assessment combined a quantitative comparison of vulnerability classes across elevation ranges with a qualitative examination of the spatial relationship between high-vulnerability areas and major coastal geomorphological and hydrological features. This integrated approach was used to evaluate the spatial coherence and physical plausibility of the FCVI results across the three climate change scenarios.

4. Results

4.1 Exposure Index

A comparative analysis of the coastal exposure index under the three climate scenarios (SSP1-2.6, SSP2-4.5, and SSP5-8.5) indicates that, although the total extent of the coastal zone remains constant across all scenarios, the spatial structure of exposure and the distribution of its classes undergo substantial reconfiguration (Figure 4a–c). This pattern suggests that the coastal system's response to increasing climatic stressors is not linear but rather emerges through nonlinear and threshold-driven dynamics. In other words, changes are not primarily expressed through a uniform increase in overall exposure but rather through a spatial redistribution of risk among exposure classes.

From a quantitative perspective, the results show that the "very low" exposure class maintains a relatively stable

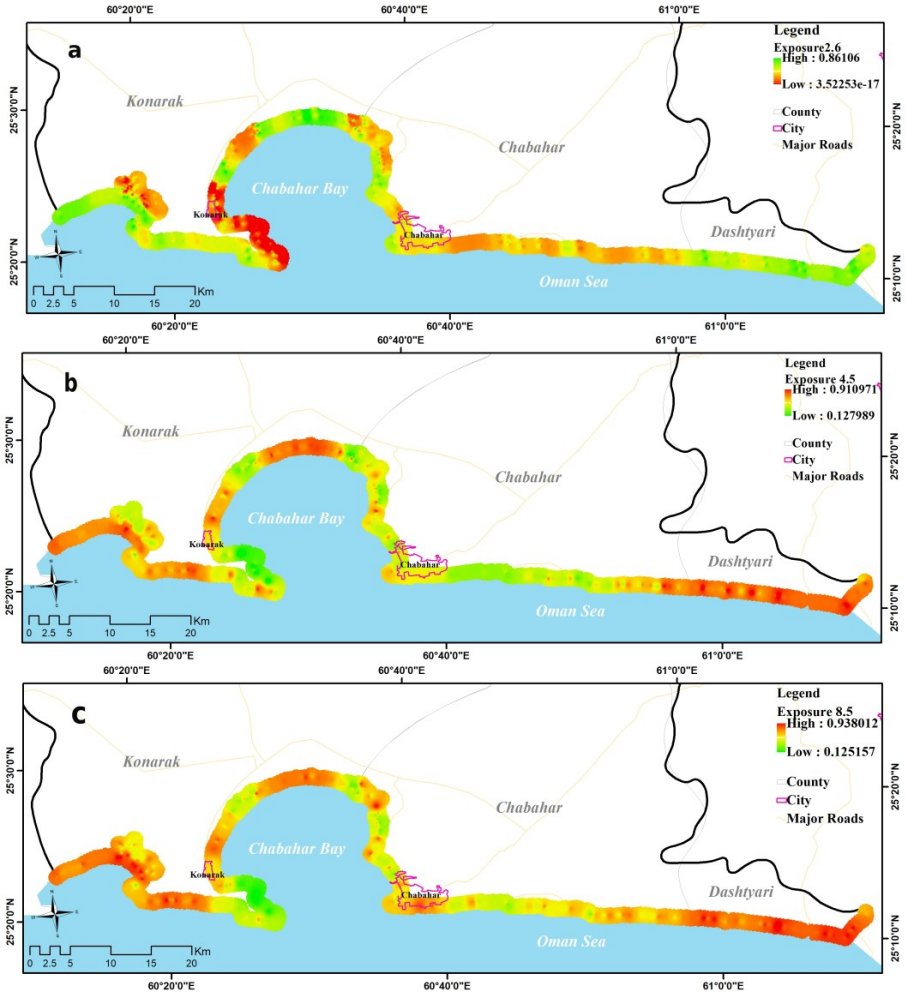


Figure 4. Spatial distribution of the Exposure Index along the Chabahar coastal zone. Warm colors indicate high exposure, whereas cool colors indicate low exposure.

area across all scenarios. This stability may reflect the presence of coastal segments with inherently higher resilience to climatic changes, which exhibit minimal variation in exposure levels across different forcing conditions. Similarly, the "very high" exposure class also shows limited variation, indicating the existence of structurally exposed zones with persistently high baseline risk that remain in the highest exposure category even under optimistic scenarios.

In contrast, the most pronounced scenario-dependent variations are observed in the intermediate classes, particularly the "low," "moderate," and "high" categories. The transition from SSP1-2.6 to SSP2-4.5 is characterized by a gradual shift of areas from the "moderate" class toward the "low" class, suggesting that the coastal system is entering a transitional threshold phase. At the same time, the gradual expansion of the "high" exposure class indicates the initial intensification of climatic pressures and a progressive weakening of the exposure system's structural equilibrium (Figure 4b).

However, the difference between SSP2-4.5 and SSP5-8.5 is more profound and structural in nature. During this transition, the area of the "low" exposure class experiences a sharp decline, while the "high" exposure class shows a marked and abrupt expansion, becoming the dominant class across the coastal zone (Figure 4c). This shift indicates that under the high-emission SSP5-8.5 scenario, the coastal system enters a rapid risk escalation regime, in which areas characterized by low or moderate exposure are directly and quickly reclassified into high-exposure conditions.

The expansion of high-exposure zones under SSP5-8.5 further suggests an increased likelihood of spatial co-occurrence and overlap of coastal hazards at the regional scale. It also indicates that large portions of the coastline would transition into persistently high and unstable exposure states under this scenario. Overall, the findings clearly demonstrate that the primary difference between optimistic and pessimistic scenarios does not lie in a gradual increase in coastal exposure but rather in the collapse of low-risk structures and the rapid dominance of high-

exposure classes. This highlights the limitations of linear trend-based planning approaches and underscores the necessity of incorporating nonlinear and threshold-based dynamics into coastal risk assessment and management frameworks.

4.2 Sensitivity Index

As illustrated in Figure 5(a–e), the spatial distribution of socioeconomic indicators related to sensitivity, as well as the final composite Sensitivity Index, reveals pronounced spatial heterogeneity along the coastal zone. The values of these indicators exhibit distinct spatial patterns, reflecting substantial differences in population pressure, urban development intensity, economic dependence, and the distribution of vulnerable communities across different coastal segments.

The agricultural sector GDP indicator shows higher levels of economic sensitivity in specific coastal areas with greater dependence on agricultural activities. These regions are characterized by elevated index values and display a clearly identifiable clustered spatial pattern. The population density indicator reveals increased sensitivity values along densely populated coastal corridors. High population concentrations in these areas result in zones with elevated index values, highlighting a clear distinction between low- and high-density coastal regions.

Urbanized areas also exhibit an uneven spatial distribution along the coastline. Regions with higher levels of urbanization show a distinct spatial concentration of elevated sensitivity values, reflecting the pattern of urban expansion in coastal zones. In addition, the distribution of socially vulnerable population groups is spatially heterogeneous, with certain coastal segments characterized by higher concentrations of these groups. These areas are identified as zones of increased social sensitivity within the framework of the indicators used.

Finally, the composite Sensitivity Index, derived from the integration of socioeconomic components, presents an integrated spatial pattern of sensitivity across the coastal zone and identifies hotspots with higher index values, reflecting the spatial overlap of multiple sensitivity drivers.

4.3 Spatial pattern of the Sensitivity Index

The spatial analysis of the Sensitivity Index along the study coastline reveals considerable heterogeneity in its distribution. As shown in Figure 6, the highest sensitivity values (up to 0.339, represented by red to orange classes) are predominantly concentrated in the central coastal segment, particularly in the vicinity of Chabahar City. This pattern indicates a direct relationship between increased coastal sensitivity and the intensity of human activities, urban development, and proximity to major transportation networks and infrastructure systems.

In contrast, the eastern and western sections of the coastline are mainly characterized by low to moderate sensitivity levels (green to yellow classes), reflecting relatively stable environmental conditions and lower anthropogenic pressure in these areas. The gradual spatial variation in sensitivity values along the coastline highlights the combined influence of natural coastal processes and human interventions on system vulnerability, emphasizing the complex spatial response of coastal environments to environmental stressors.

Overall, the results demonstrate that coastal segments located near urban centers and major access routes exhibit significantly higher sensitivity than other areas. Consequently, these zones should be prioritized in integrated coastal zone management strategies, continuous monitoring programs, and risk reduction planning. The identification of high-sensitivity areas provides a robust scientific basis for evidence-based decision-making and contributes to enhancing the resilience of coastal systems.

4.4 Adaptive Capacity Index

The analysis of the adaptive capacity maps presented in Figure 7(a–e) indicates that the spatial distribution of the main components of adaptive capacity, including education level, per capita gross domestic product (GDP), medical services, and transportation infrastructure, exhibits pronounced spatial heterogeneity along the Chabahar coastal zone. These patterns reflect a structural concentration of these indicators within urban areas, accompanied by a gradual decline toward peripheral and less-developed coastal regions.

As shown in Figure 7d, the education index reaches its highest values within the urban area of Chabahar and parts of the central region of the study area. In contrast, a gradual and significant decrease in this indicator is observed along the eastern coastal segments and in areas located farther from population centers, indicating more limited access to educational infrastructure and services in these regions.

Similarly, as shown in Figure 7c, the per capita GDP index exhibits higher values predominantly around Chabahar City and in areas characterized by concentrated economic, commercial, and infrastructural activities. In contrast, less-developed coastal areas, particularly in the eastern part of the study region, exhibit lower values of this indicator. This spatial pattern clearly highlights existing socioeconomic disparities and underscores the pivotal role of urban centers in enhancing adaptive capacity within the coastal system.

Consistent with Figure 8, the Adaptive Capacity Index along the Chabahar coastal zone exhibits pronounced spatial heterogeneity. Higher values of the index are mainly concentrated around the urban core of Chabahar and the central coastal segments, reflecting the accumulation of infrastructural capacity, public services, and socioeconomic resources in these areas. In contrast, the eastern coastal areas, particularly within the Dashtiari region, are characterized by lower adaptive capacity values, indicating comparatively limited capacity to adapt to coastal hazards.

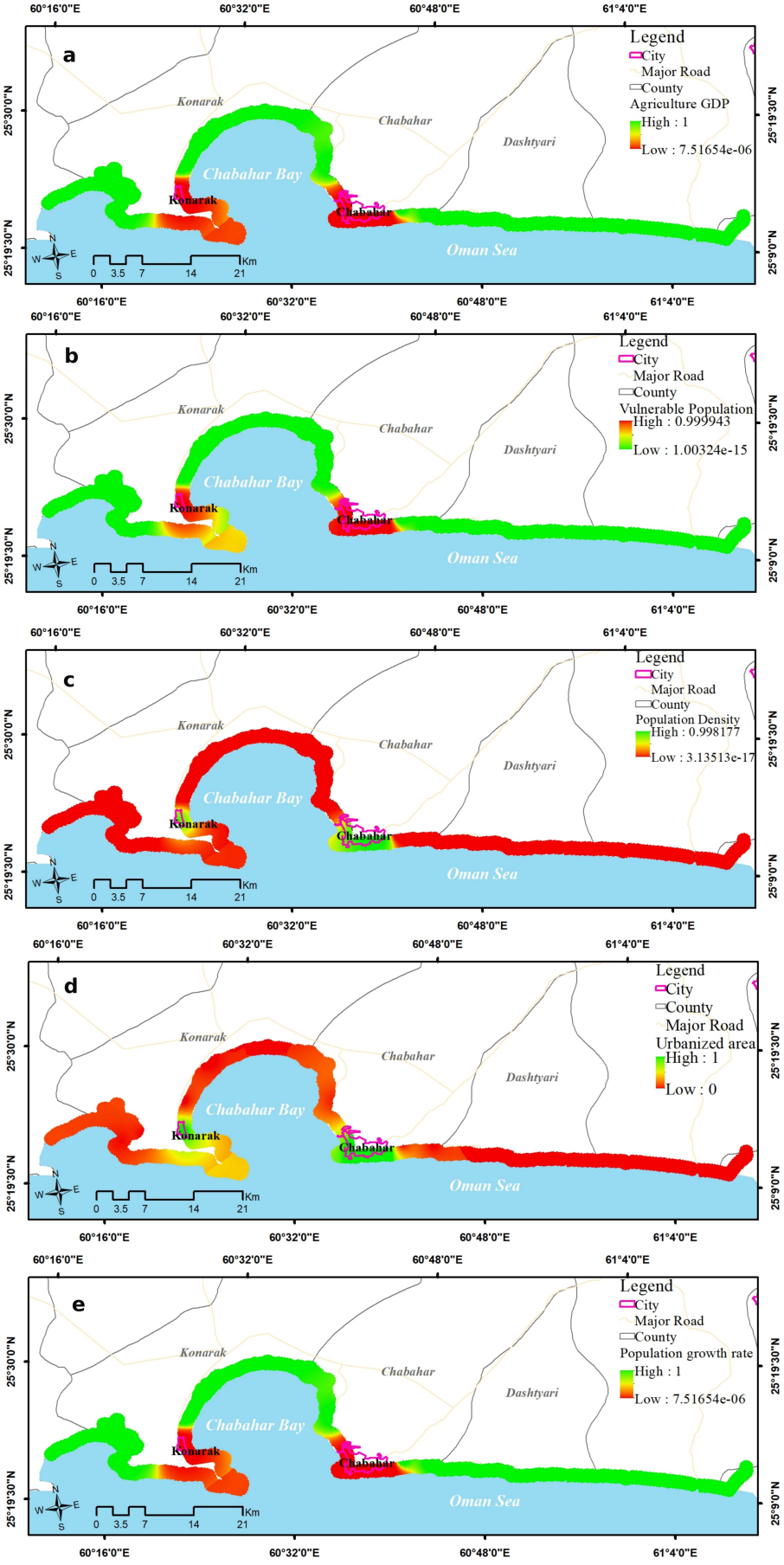


Figure 5. Spatial patterns of socio-economic sensitivity indicators used in this study, including: a) agricultural GDP, b) population density, c) vulnerable population, and d) urbanized areas. Panel e) shows the population growth rate.

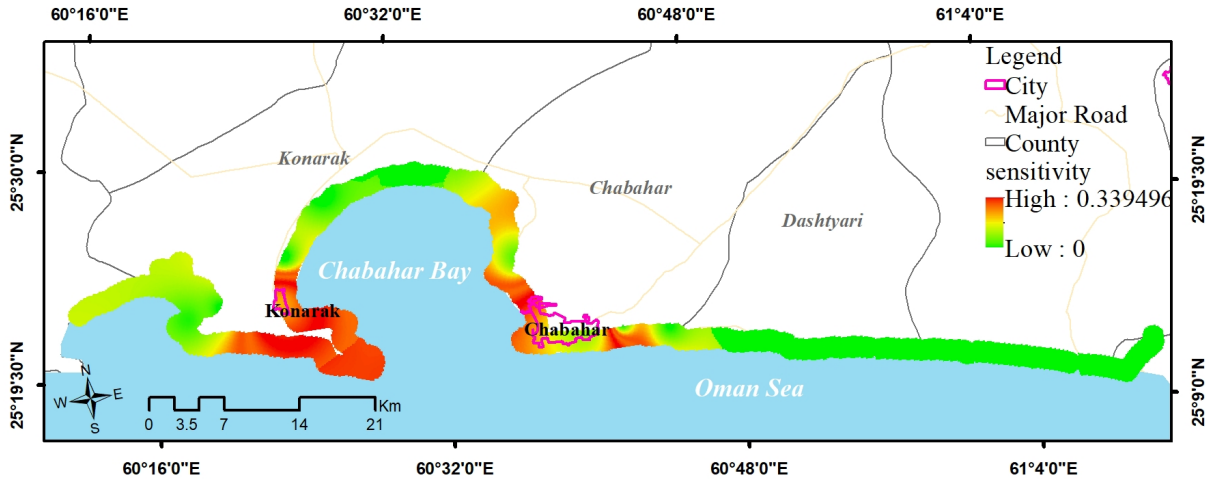


Figure 6. Spatial distribution of the Sensitivity Index along the study coastline, showing spatial heterogeneity in sensitivity values and the concentration of high-sensitivity zones in the central coastal segments.

Overall, the results presented in Figure 8 highlight an uneven spatial distribution of adaptive capacity, with a clear concentration in urban hubs and a gradual decline toward peripheral coastal zones.

The spatial distribution of the Coastal Adaptability Index reveals considerable heterogeneity along the Chabahar coastline. Higher index values are predominantly concentrated within Chabahar Bay and in areas adjacent to urban settlements, whereas the open and continuous coastal stretches in the eastern part of the region are mainly characterized by lower values. The spatial pattern of the index indicates a concentration of higher-adaptability zones within the inner-bay areas and a gradual decrease in index values toward the open coasts of the Sea of Oman.

4.5 Final climate scenarios of the Coastal Vulnerability Index (FCVI)

The quantitative analysis of the Fuzzy Composite Coastal Vulnerability Index (FCVI) under the SSP1-2.6, SSP2-4.5, and SSP5-8.5 scenarios reveals significant changes in the areal composition of vulnerability classes across the study coastline (Table 2; Figure 9a–c).

Under the low-emission SSP2-6 scenario, the largest proportion of the coastal zone falls within the "very low vulnerability" class, while high and very high vulnerability classes occupy a relatively limited extent. Intermediate classes account for a considerable share of the study area, indicating the dominance of low-risk conditions alongside the presence of transitional zones.

With the increase in scenario intensity to SSP4.5, the spatial distribution of FCVI classes undergoes a noticeable reconfiguration. The proportion of low-vulnerability areas decreases, accompanied by an expansion in the "low," "high," and "very high" vulnerability classes. This shift indicates a gradual spatial spread of higher vulnerability zones compared to the SSP2-6 scenario, reflecting an intensification of climate-driven pressures across the coastal system.

Under the high-emission SSP5-8.5 scenario, the proportion of the high-vulnerability classes remains substantial. In this scenario, the combined area of the "high" and "very high" vulnerability classes constitutes a considerable portion of the coastal zone, whereas the share of the "very low vulnerability" class decreases compared with the lower-intensity scenarios. These results indicate a gradual reconfiguration of the areal composition of coastal vulnerability with increasing climate scenario severity.

The quantitative patterns presented in Table 2 are directly reflected in the scenario-based coastal vulnerability maps. As shown in Figure 9, the reduction in low-vulnerability classes and the increase in high-vulnerability areas observed in the numerical results are spatially manifested through the expansion and increased continuity of high-vulnerability zones along the coastline.

Table 2. Area distribution of Fuzzy Composite Coastal Vulnerability Index (FCVI) classes under different climate scenarios.

Vulnerability class	Value	SSP8.5 (ha)	SSP4.5 (ha)	SSP2.5 (ha)
Very low	1	1,108,327	1,096,947	1,315,095
Low	2	706,912	752,582	444,277
Moderate	3	420,038	488,025	616,608
High	4	521,574	498,223	396,095
Very high	5	449,598	462,012	480,044
Total area	–	3,252,118	3,252,118	3,252,118

Under the SSP1-2.6 scenario, the dominance of low-vulnerability classes in the quantitative results is consistent with a fragmented and localized distribution of high-risk patches in the spatial maps. In contrast, under SSP2-4.5 and particularly SSP5-8.5, the increasing share of the "high" and "very high" vulnerability classes is spatially ex-

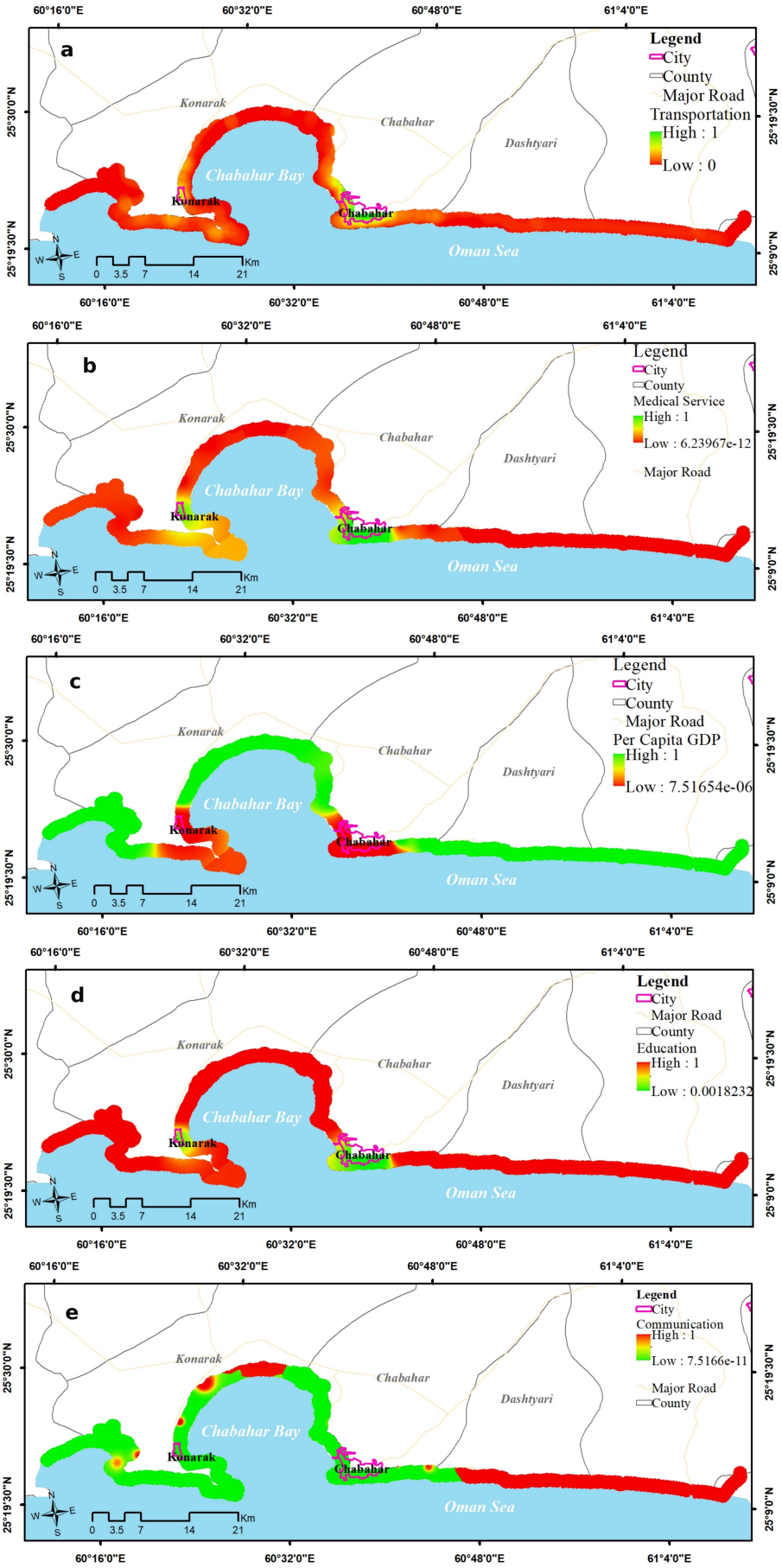


Figure 7. Spatial distribution of socioeconomic components along the Chabahar coastal zone: a) transportation, b) medical services, c) per capita GDP, d) education level, and e) communications.

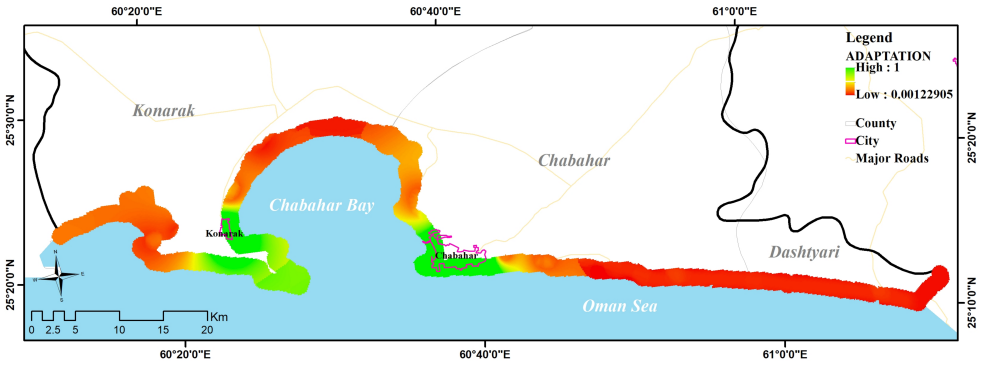


Figure 8. Spatial distribution of the Coastal Adaptability Index along the Chabahar coastal zone.

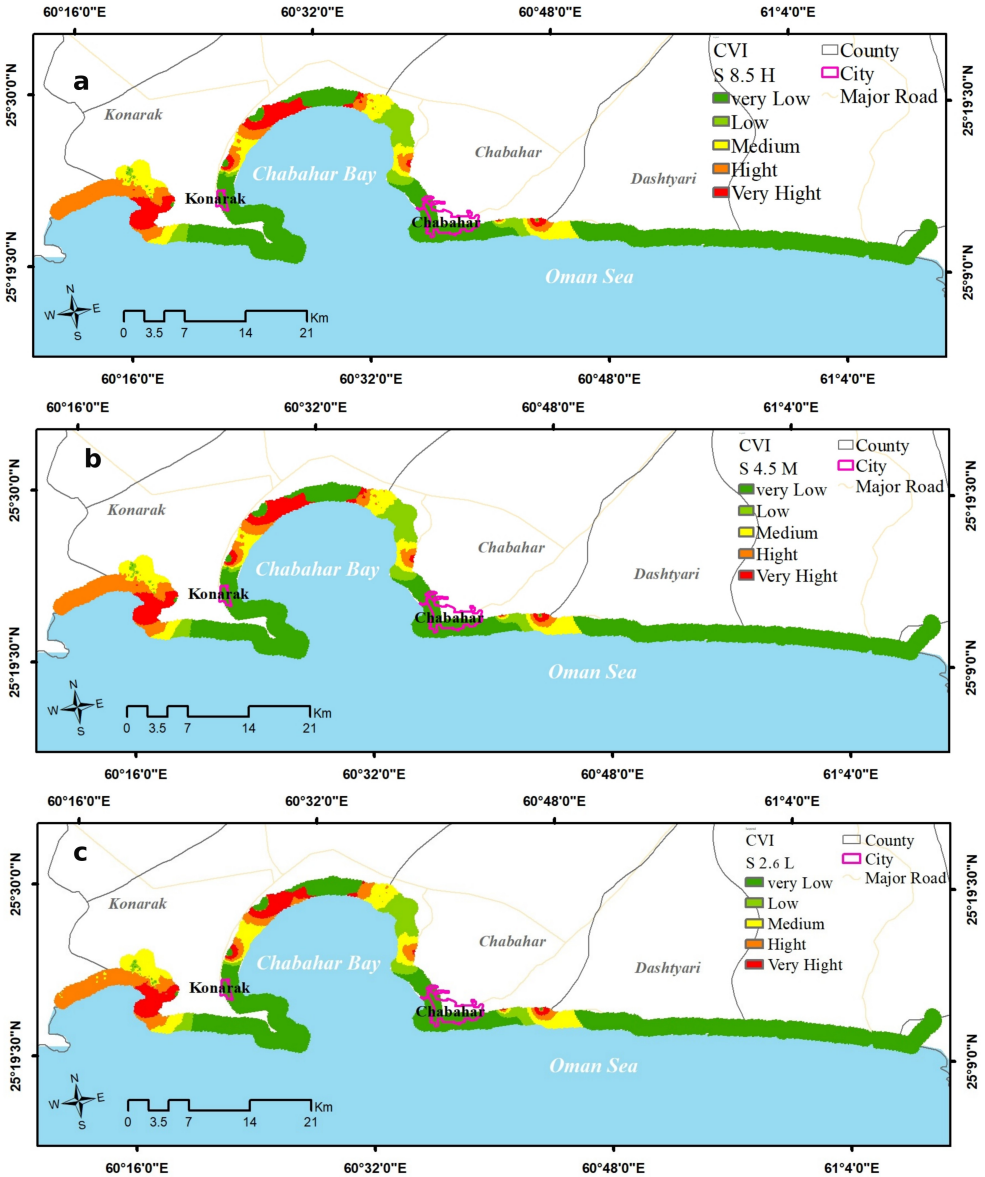


Figure 9. Spatial distribution of the Fuzzy Composite Coastal Vulnerability Index (FCVI) along the Chabahar and Konarak coasts under the SSP5-8.5 (a), SSP2-4.5 (b), and SSP1-2.6 (c) scenarios, showing the increasing extent and spatial continuity of high-vulnerability zones under higher-emission scenarios.

Table 3. Elevation-based spatial consistency assessment of coastal vulnerability maps under future climate scenarios.

Elevation Class (m)	Total Elevation Points (n)*	SSP1-2.6		SSP2-4.5		SSP5-8.5	
		Points (n)	Percentage (%)	Points (n)**	Percentage (%)***	Points (n)**	Percentage (%)***
≤ 0	1,419	1,022	72.00	984	69.34	977	68.85
0–1	1,192	868	72.80	890	74.66	911	76.42
1–5	6,460	4,089	63.29	4,509	69.79	4,480	69.34
Total	9,071	5,979	65.93	6,383	70.34	6,368	–

*Total Elevation Points (n): Total number of DEM pixels within each elevation class.
**Points (n): Number of vulnerable pixels classified as High or Very High within each elevation class.
***Percentage (%): Percentage of vulnerable pixels relative to the total number of pixels within the corresponding elevation class.

pressed through the formation of more continuous and extensive high-vulnerability belts and corridors.

This numerical–spatial consistency demonstrates that changes in the areal composition of FCVI classes are accompanied by a clear spatial reorganization of coastal vulnerability patterns, highlighting a strong coupling between quantitative shifts and spatial restructuring of coastal risk.

4.6 Spatial patterns of scenario-based FCVI maps

The scenario-based maps of the Fuzzy Composite Coastal Vulnerability Index (FCVI) illustrate spatial variations in the distribution of vulnerability classes under different climate scenarios along the Chabahar coastline (Figure 9). These maps indicate that, with increasing climate scenario intensity, the spatial pattern of vulnerability shifts from more fragmented configurations toward increasingly consolidated and spatially continuous patterns. Under the SSP1-2.6 scenario, the spatial pattern of the FCVI is largely dominated by the "very low" and "low" vulnerability classes. High- and very-high-vulnerability areas are distributed in a patchy, limited, and discontinuous manner, primarily concentrated in the western part of the study area and in certain segments around Chabahar Bay. In contrast, extensive areas along the eastern coastline, particularly within the Dashtiari region, fall within the low-vulnerability classes.

Under the SSP2-4.5 scenario, an expansion of the "moderate" and "high" vulnerability classes is observed around Chabahar Bay and in parts of the eastern coastline. Compared with SSP1-2.6, high-vulnerability zones exhibit greater spatial continuity and, in some coastal segments, form more elongated and coherent patterns. At the same time, the extent of very-low-vulnerability areas decreases, and the overall spatial configuration of the FCVI becomes more compact.

Under the SSP5-8.5 scenario, the spatial transformation of the FCVI becomes more pronounced. In this scenario, the "high" and "very high" vulnerability classes expand across large portions of the coastline and, in some areas, particularly around Chabahar Bay and parts of the western coastline, become the dominant spatial pattern. High-vulnerability zones transition from fragmented patches into more continuous belts and corridors, while the extent of very-low-vulnerability areas declines significantly.

Overall, the combined quantitative and spatial results of the Fuzzy Composite Coastal Vulnerability Index (FCVI) demonstrate that, with increasing climate forcing from SSP1-2.6 to SSP5-8.5, both the areal composition and spatial configuration of vulnerability classes undergo gradual yet significant transformation. These changes are characterized by a reduction in low-vulnerability areas and a simultaneous increase in both the extent and spatial continuity of high-vulnerability zones across the coastal landscape.

4.7 Validation Results Based on Elevation Classes

The validation results demonstrated that, across all climate scenarios, more than 63% of the validation points within the low-elevation classes (≤ 5 m) were classified as High or Very High vulnerability. The highest level of spatial agreement was achieved under the SSP2-4.5 scenario (70.34%), followed by SSP5-8.5 (70.20%) and SSP1-2.6 (65.93%). This strong correspondence indicates that the proposed vulnerability model successfully captured the spatial concentration of vulnerability in low-lying coastal areas, which are inherently more exposed and sensitive to coastal hazards (Table 3).

The results of this study indicate that coastal vulnerability patterns along the Makran coast are strongly dependent on the intensity of climate change scenarios. The observed variations in both the areal composition and spatial continuity of vulnerability classes demonstrate that the coastal system's response to increasing climatic pressure goes beyond a gradual increase in vulnerability magnitude and is instead accompanied by a structural reorganization of spatial patterns. These findings provide a meaningful basis for interpreting the roles of physical, socioeconomic, and ecological drivers in shaping coastal vulnerability.

The spatial patterns of coastal sensitivity and exposure along the Chabahar coastline result from the interaction of physical, socioeconomic, and ecological factors. The spatial clustering of high-sensitivity zones in densely populated and urbanized areas is consistent with a growing body

of literature emphasizing the critical role of population concentration, asset density, and urban development pathways in amplifying climate-related impacts (Birkmann et al., 2022; IPCC, 2022). In this context, coastal settlements are not only exposed to physical hazards but also exhibit reduced adaptive capacity due to institutional, economic, and infrastructural constraints (Hinkel et al., 2018; Oppenheimer et al., 2019).

From a methodological perspective, the findings underscore the need to reconsider the structure of traditional coastal vulnerability indices. While classical coastal vulnerability approaches have been effective in identifying spatial patterns of vulnerability based primarily on geomorphological and physical variables (Gornitz, 1991; Thieler and Hammar-Klose, 2000), recent studies have highlighted their limitations in adequately representing human sensitivity and socioeconomic inequalities (Nguyen et al., 2021; Bevacqua et al., 2023). The comprehensive review by ElKotby (2026) further indicates that, in a substantial proportion of coastal vulnerability studies, socioeconomic components are either partially incorporated or assigned a secondary role. In this regard, the simultaneous integration of population density, urbanization, vulnerable population groups, and economic dependency in this study provides a more realistic representation of human sensitivity and aligns with recent advances toward integrated vulnerability frameworks such as ICVI and SVI (Cutter et al., 2003; Rocha et al., 2023).

The spatial pattern analysis of exposure under different climate scenarios reveals pronounced spatial heterogeneity and a strong dependence of exposure on future emission pathways. Under the low-emission scenario, exposure remains relatively limited and spatially patchy, whereas with increasing scenario intensity, both the extent and spatial continuity of high-exposure zones increase. This transition from dispersed exposure to more continuous spatial clusters, particularly along the eastern coast of Chabahar, is consistent with global studies emphasizing the roles of sea-level rise, intensification of extreme sea levels, and changes in coastal flood hazard under future climate conditions (Vousdoukas et al., 2018; Kirezci et al., 2020; Tebaldi et al., 2021).

Studies of coastal flood risk indicate that the combined effects of sea-level rise, extreme sea levels, wave forcing, storm surges, and vertical land movements can substantially amplify coastal flood exposure and risk (Vousdoukas et al., 2018; Nicholls et al., 2021). Within this context, the spatial patterns observed in this study can be interpreted as reflecting the combined influence of geomorphological characteristics, low coastal elevation and slope, and limited natural buffering capacity. These factors are particularly important in determining the spatial distribution of coastal vulnerability, with global assessments indicating that tropical and subtropical regions generally exhibit higher coastal vulnerability and that geomorphology and coastal slope are among the dominant contributors to coastal vulnerability (Basnayake et al., 2026).

A key finding of this study is the transformation of exposure patterns from fragmented hotspots into spatially connected corridors and coastal belts under high-emission scenarios. This pattern may reflect a nonlinear response of the coastal system to intensified climatic forcing, whereby sea-level rise acts as a background driver that simultaneously activates thresholds for inundation and erosion, leading to a spatial reorganization of exposure patterns (IPCC, 2021; Haasnoot et al., 2020). Such transformations highlight the importance of spatially explicit and scenario-based analyses for long-term adaptation planning, as the concentration of risk in specific hotspots may generate disproportionate socioeconomic impacts.

Finally, the results are consistent with studies emphasizing the role of nature-based solutions in reducing exposure and enhancing coastal resilience. Evidence suggests that ecosystems such as mangrove forests, coastal wetlands, and tidal flats can significantly attenuate wave energy and reduce the intensity of coastal flooding (Narayan et al., 2017; Reguero et al., 2018; Menéndez et al., 2020). Accordingly, the degradation or loss of these systems can be considered a key driver of increasing exposure and vulnerability in critical coastal zones.

The scenario-based maps of the Fuzzy Composite Coastal Vulnerability Index (FCVI) developed in this study provide a spatial decision-support tool for integrated coastal zone management. These outputs identify where and under which climatic pathways the transition from fragmented risks to continuous high-risk zones occurs. Accordingly, they can be used for: (i) coastal zoning and land-use regulation through the definition of restricted development corridors in highly vulnerable areas; (ii) prioritization of interventions by allocating resources to transitional hotspots that emerge under SSP2-4.5 but evolve into dominant high-vulnerability zones under SSP5-8.5; and (iii) designing place-based adaptation strategies that combine engineering measures with nature-based solutions, such as coastal ecosystem conservation and restoration. This approach not only reduces the risk of maladaptive infrastructure investments in high-risk zones but also enables the development of phased and scenario-based adaptation packages for the Chabahar and Konarak coastal regions.

The effectiveness of these management measures, however, also depends on the extent to which the interests, knowledge, and priorities of relevant stakeholders are incorporated into subsequent planning and decision-making processes. In the context of Integrated Coastal Zone Management (ICZM), the spatial information provided by the FCVI can support dialogue and coordination among governmental institutions, provincial and local authorities, coastal communities, resource users, and other relevant stakeholders. The identification of high- and very-high-vulnerability areas can provide a common spatial evidence

base for discussing management priorities, evaluating alternative adaptation options, and allocating resources. Stakeholder participation was not directly incorporated into the FCVI modeling process in the present study. Rather, the FCVI is intended to complement participatory coastal planning by providing spatial evidence that can inform subsequent stakeholder engagement, prioritization, and implementation of coastal management measures. Incorporating stakeholder knowledge and preferences into the prioritization and implementation of these measures therefore represents an important direction for future research and practical application.

5. Conclusion

This study, through the development and application of an integrated framework based on fuzzy logic, makes a significant contribution to improving coastal vulnerability assessment under conditions of climatic uncertainty and increasing human pressure. The results demonstrate that coastal vulnerability along the Makran coast is not a static or unidimensional phenomenon but rather the outcome of a complex and nonlinear interaction among physical exposure, socioeconomic sensitivity, and the adaptive capacity of coastal communities. Under more severe climate scenarios, this interaction leads to a fundamental reconfiguration of the spatial structure of vulnerability.

The scenario-based analysis of the Fuzzy Composite Coastal Vulnerability Index (FCVI) reveals that the main difference between optimistic and pessimistic climate pathways is not merely a gradual increase in vulnerability magnitude but rather a shift in the "spatial regime" of the coastal system's response. Under low-emission scenarios, vulnerability remains largely patchy, fragmented, and spatially limited, whereas under the high-emission SSP5-8.5 scenario, extensive and spatially continuous high-vulnerability zones emerge. This indicates that the coastal system crosses spatial thresholds and transitions into more unstable configurations. Such patterns suggest that coastal systems respond to intensified climatic stress in a nonlinear and threshold-dependent manner that cannot be adequately captured through linear or mean-based approaches.

From a methodological perspective, the findings highlight the efficiency and necessity of fuzzy-based approaches for integrating heterogeneous physical, socioeconomic, and ecological variables. The proposed FCVI framework enables the simultaneous integration of exposure, sensitivity, and adaptive capacity, thereby overcoming key limitations of traditional physically oriented coastal vulnerability indices and providing a more realistic representation of spatial vulnerability patterns. This approach is particularly relevant for dynamic regions such as the Makran coast, where climatic uncertainty, geomorphological diversity, and socioeconomic pressures coexist.

From an applied perspective, the identification of persistent vulnerability hotspots and corridors along the Chabahar and Konarak coasts provides a scientific basis for prioritizing interventions, targeting place-based adaptation policies, and strengthening integrated coastal zone management. The results indicate that relying solely on structural or reactive measures, without considering socioeconomic capacity and ecosystem services, cannot lead to sustainable risk reduction. In this context, combined strategies, including the protection and restoration of coastal ecosystems, enhancement of social infrastructure, and strengthening of institutional capacity, play a central role in improving coastal system resilience.

Finally, this study demonstrates that the transition from traditional vulnerability indices to integrated and scenario-based frameworks is not merely a methodological choice but a scientific necessity for addressing the complex challenges of climate change in coastal regions. The proposed framework can serve as a foundation for future research, multi-hazard assessments, and strategic decision-making in other similar coastal environments, thereby contributing to the advancement of applied knowledge in coastal climate risk management. With minimal data modification, the framework also has strong potential for transferability to other developing coastal regions with comparable geomorphological and socioeconomic characteristics.

CRediT authorship contribution statement

Faeze Chehrazar contributed to conceptualization, methodology, formal analysis, investigation, data curation, software, validation, visualization, and writing of the original draft. Esmail Salehi contributed to conceptualization, methodology, supervision, project administration, and writing review and editing. Ahmad Nohegar contributed to methodology, validation, formal analysis, and writing review and editing. María-José Prados contributed to conceptualization, interpretation of results, and writing. Majid Habibi Nokhandan contributed to resources.

Funding

This research was supported by the Iran National Science Foundation (INSF) under grant number 4026190.

Conflict of interest

None declared.

References

Abijith, D., Saravanan, S., Sundar, P.K.S., 2023. *Coastal vulnerability assessment for the coast of Tamil Nadu, India: a geospatial approach*. Environ. Sci. Pollut. Res. 30, 75610–75628. https://doi.org/10.1007/s11356-023-27686-8

Akash, S.H., Sarkar, S.K., Bindajam, A.A., Kumari, R., Talukdar, S., Mallick, J., 2024. *Assessment of coastal vulnerability using integrated fuzzy analytical hierarchy process and geospatial technology for effective coastal management*. Environ. Sci. Pollut. Res. 31, 53749–53766. https://doi.org/10.1007/s11356-023-28317-y

Alcántara-Carrió, J., García Echavarría, L.M., Jaramillo-Vélez, A., 2024. *Is the coastal vulnerability index a suitable indexsuitable? Review and proposal of alternative indices for coastal vulnerability to sea level rise*. Geo-Mar. Lett. 44, 8. https://doi.org/10.1007/s00367-024-00770-9

Arkema, K.K., Guannel, G., Verutes, G., Wood, S.A., Guerry, A., Ruckelshaus, M., Kareiva, P., Lacayo, M., Silver, J.M., 2013. *Coastal habitats shield people and property from sea-level rise storms*. Nat. Clim. Change 3, 913–918. https://doi.org/10.1038/nclimate1944

Arun Kumar, A., Kunte, P.D., 2012. *Coastal vulnerability assessment for Chennai, east coast of India using geospatial techniques*. Nat. Hazards 64, 853–872. https://doi.org/10.1007/s11069-012-0276-4

Basnayake, V., Duong, T.M., Ranasinghe, R., Almar, R., Wijnberg, K.M., 2026. *A global assessment of coastal, vulnerability and dominant contributors*. Nat. Commun. 17, 578. https://doi.org/10.1038/s41467-025-67275-6

Bevacqua, E., Suárez-Gutiérrez, L., Jézéquel, A., Lehner, F., Vrac, M., Yiou, P., Zscheischler, J., 2023. *Advancing research on compound weather and climate events via large ensemble model simulations*. Nat. Commun. 14, 2145. https://doi.org/10.1038/s41467-023-37847-5

Bevacqua, E., Vousdoukas, M.I., Zappa, G., Hodges, K., Shepherd, T.G., Maraun, D., Mentaschi, L., Feyen, L., 2020. *More meteorological events that drive compound coastal flooding are projected under climate change*. Commun. Earth Environ. 1, 47. https://doi.org/10.1038/s43247-020-00044-z https://doi.org/10.1038/s43247-020-00044-0

Birkmann, J., Liwenga, E., Pandey, R., Boyd, E., Djalante, R., Gemenne, F., Leal Filho, W., Pinho, P.F., Stringer, L., Wrathall, D., 2022. *Poverty, livelihoods and sustainable development*. In: Pörtner, H.-O., Roberts, D.C., Tignor, M., Poloczanska, E.S., Mintenbeck, K., Alegría, A., Craig, M., Langsdorf, S., Löschke, S., Möller, V., Okem, A., Rama, B. (Eds.), *Climate Change 2022: Impacts, Adaptation and Vulnerability*, Contribution of Working Group II to the Sixth Assessment Report of the Intergovernmental Panel on Climate Change. Cambridge Univ. Press, 1171–1274. https://doi.org/10.1017/9781009325844.010

Boumpoulis, V., Depountis, N., Dimas, A., Papatheodorou, G., 2025. *Presentation and analysis of the Geotechnical Coastal Vulnerability Index and validation of its application to coastal erosion problems*. Sci. Rep. 15, 1424. https://doi.org/10.1038/s41598-025-85594-y

Cruz-Ramírez, C.J., Chávez, V., Silva, R., Muñoz-Pérez, J.J., Rivera-Arriaga, E., 2024. *Coastal management: A review of key elements for vulnerability assessment*. J. Mar. Sci. Eng. 12, 386. https://doi.org/10.3390/jmse12030386

Cutter, S.L., Boruff, B.J., Shirley, W.L., 2003. *Social vulnerability to environmental hazards*. Soc. Sci. Q. 84, 242–261. https://doi.org/10.1111/1540-6237.8402002

Cutter, S.L., Finch, C., 2008. *Temporal and spatial changes in social vulnerability to natural hazards*. Proc. Natl. Acad. Sci. U.S.A. 105, 2301–2306. https://doi.org/10.1073/pnas.0710375105

Dasgupta, S., Laplante, B., Meisner, C., Wheeler, D., Yan, J., 2009. *The impact of sea level rise on developing countries: A comparative analysis*. Clim. Change 93, 379–388. https://doi.org10.1007/s10584-008-9499-5

Deb, D., Uddin, M.M., Mahbub-E-Kibria, A.S.M., Das, M.K., Hasan, M., 2024. *Coastal vulnerability assessment to multi hazardsmulti-hazards in the exposed coast of the Southeastern Coastal Region of Bangladesh*. Reg. Stud. Mar. Sci. 73, 103484. https://doi.org/10.1016/j.rsma.2024.103484

ElKotby, M.R., 2026. *Progression in Coastal Vulnerability Index (CVI) approaches for assessing risk: A comprehensive review*. J. Afr. Earth Sci. 234, 105917. https://doi.org/10.1016/j.jafrearsci.2025.105917

ElKotby, M.R., Sarhan, T.A., El-Gamal, M., Masria, A., 2024. *Evaluation of coastal risks to sea level rise: Case study of Nile Delta Coast*. Reg. Stud. Mar. Sci. 78, 103791. https://doi.org/10.1016/j.rsma.2024.103791

Gesch, D.B., 2018. *Best practices for elevation-based assessments of sea-level rise and coastal flooding exposure*. Front. Earth Sci. 6, 230. https://doi.org/10.3389/feart.2018.00230

Ghaderi, D., Rahbani, M., 2024. *Evaluating the shoreline vulnerability of the eastern coast of Makran employing geomorphological and hydrodynamic parameters*. J. Earth Syst. Sci. 133, 48. https://doi.org/10.1007/s12040-024-02266-7

Gornitz, V., 1991. *Global coastal hazards from future sea level rise*. Palaeogeogr. Palaeoclimatol. Palaeoecol. 89, 379–398. https://doi.org/10.1016/0031-0182(91)90173-O

Government of the Islamic Republic of Iran, 1993. *Act on the Marine Areas of the Islamic Republic of Iran in the Persian Gulf and the Oman Sea*.

Haasnoot, M., Kwakkel, J.H., Walker, W.E., ter Maat, J., 2013. *Dynamic adaptive policy pathways: A method for crafting robust decisions for a deeply uncertain world*. Glob. Environ. Change 23, 485–498. https://doi.org/10.1016/j.gloenvcha.2012.12.006

Hinkel, J., 2011. *Indicators of vulnerability and adaptive capacity: Towards a clarification of the science-policy*

interface. Glob. Environ. Change 21, 198–208. https://doi.org/10.1016/j.gloenvcha.2010.08.002

Hinkel, J., Aerts, J.C.J.H., Brown, S., Jiménez, J.A., Lincke, D., Nicholls, R.J., Scussolini, P., Sanchez-Arcilla, A., Vafeidis, A.T., Appeaning Addo, K., 2018. *The ability of societies to adapt to twenty-first-century sea-level rise*. Nat. Clim. Change 8, 570–578. https://doi.org/10.1038/s41558-018-0176-z

Hinkel, J., Klein, R.J.T., 2009. *Integrating knowledge to assess coastal vulnerability to sea-level rise: The development of the DIVA tool*. Glob. Environ. Change 19, 384–395. https://doi.org/10.1016/j.gloenvcha.2009.03.002

Hooijer, A., Vernimmen, R., 2021. *Global LiDAR land elevation data reveal greatest sea-level rise vulnerability in the tropics*. Nat. Commun. 12, 3592. https://doi.org/10.1038/s41467-021-23810-9

Hoque, M.A.A., Ahmed, N., Pradhan, B., Roy, S., 2019. *Assessment of coastal vulnerability to multi-hazardous events using geospatial techniques along the eastern coast of Bangladesh*. Ocean Coast. Manag. 181, 104898. https://doi.org/10.1016/j.ocecoaman.2019.104898

IPCC, 2021. *Climate Change 2021: The Physical Science Basis*. Contribution of Working Group I to the Sixth Assessment Report of the Intergovernmental Panel on Climate Change. Cambridge Univ. Press. https://doi.org/10.1017/9781009157896

IPCC, 2022. *Climate Change 2022: Impacts, Adaptation and Vulnerability*. Contribution of Working Group II to the Sixth Assessment Report of the Intergovernmental Panel on Climate Change. Cambridge Univ. Press. https://doi.org/10.1017/9781009325844

IPCC, 2023. *Climate Change 2023: Synthesis Report*. Contribution of Working Groups I, II and III to the Sixth Assessment Report of the Intergovernmental Panel on Climate Change. IPCC. https://doi.org/10.59327/IPCC/AR6-9789291691647

Kirezci, E., Young, I.R., Ranasinghe, R., Muis, S., Nicholls, R.J., Lincke, D., Hinkel, J., 2020. *Projections of global-scale extreme sea levels and resulting episodic coastal flooding over the 21st century*. Sci. Rep. 10, 11629. https://doi.org/10.1038/s41598-020-67736-6

Mafi-Gholami, D., Zenner, E.K., Jaafari, A., Riyahi Bakhtyari, H., Tien Bui, D., 2019. *Multi-hazardsMulti-hazard vulnerability assessment of the southern coasts of Iran*. J. Environ. Manage. 252, 109628. https://doi.org/10.1016/j.jenvman.2019.109628

Mah, J.C., Penwarden, J.L., Pott, H., Theou, O., Andrew, M.K., 2023. *Social vulnerability indices: A scoping review*. BMC Public Health 23, 1253. https://doi.org/10.1186/s12889-023-16097-6

Mani Murali, R., Misra, A., Vethamony, P., 2018. *A new insight to into the vulnerability of the Central Odisha coast, India using an analytical hierarchical process (AHP) based approach*. J. Coast. Conserv. 22, 799–814. https://doi.org/10.1007/s11852-018-0610-4

Mavromatidi, A., Briche, E., Claeys, C., 2018. *Mapping and analyzing socio-environmental vulnerability to coastal hazards induced by climate change: An application to coastal Mediterranean cities in France*. Cities 72, 189–200. https://doi.org/10.1016/j.cities.2017.08.007

Menéndez, P., Losada, I.J., Torres-Ortega, S., Narayan, S., Beck, M.W., 2020. *The global flood protection benefits of mangroves*. Sci. Rep. 10, 4404. https://doi.org/10.1038/s41598-020-61136-6

Motaghi, K., Shabanian, E., Nozad-Khalil, T., 2020. *Deep structure of the western coast of the Makran subduction zone, SE Iran*. Tectonophysics 776, 228314. https://doi.org/10.1016/j.tecto.2019.228314

Mullick, M.R.A., Tanim, A.H., Islam, S.M.S., 2019. *Coastal vulnerability analysis of Bangladesh coast using fuzzy logic basedlogic-based geospatial techniques*. Ocean Coast. Manag. 174, 154–169. https://doi.org/10.1016/j.ocecoaman.2019.03.010

Narayan, S., Beck, M.W., Reguero, B.G., Losada, I.J., van Wesenbeeck, B., Pontee, N., Sanchirico, J.N., Ingram, J.C., Lange, G.-M., Burks-Copes, K.A., 2016. *The effectiveness, costs and coastal protection benefits of natural and nature-based defences*. PLoS One 11, e0154735. https://doi.org/10.1371/journal.pone.0154735

Natural Capital Alliance, Stanford University, 2026. *InVEST User Guide*. The Natural Capital Project, Stanford University. InVEST User Guide.

Neumann, B., Vafeidis, A.T., Zimmermann, J., Nicholls, R.J., 2015. *Future coastal population growth and exposure to sea-level rise and coastal flooding: A global assessment*. PLoS One 10, e0118571. https://doi.org/10.1371/journal.pone.0118571

Nicholls, R.J., Lincke, D., Hinkel, J., Brown, S., Vafeidis, A.T., Meyssignac, B., Hanson, S., 2021. *A global analysis of subsidence, relative sea-level change and coastal flood exposure*. Nat. Clim. Change 11, 338–342. https://doi.org/10.1038/s41558-021-00993-z

Oloyede, M.O., Williams, A.B., Ode, G.O., Benson, N.U., 2022. *Coastal vulnerability assessment: A case study of the Nigerian coastline*. Sustainability 14, 2097. https://doi.org/10.3390/su14042097

Oppenheimer, M., Glavovic, B.C., Hinkel, J., van de Wal, R., Magnan, A.K., Abd-Elgawad, A., Cai, R., Cifuentes-Jara, M., DeConto, R.M., Ghosh, T., Hay, J., Isla, F., Marzeion, B., Meyssignac, B., Sebesvari, Z., 2019. *Sea level rise and implications for low-lying islands, coasts and communities*. [In:] Pörtner, H.-O., Roberts, D.C., Masson-Delmotte, V., Zhai, P., Tignor, M., Poloczanska, E., Mintenbeck, K., Alegría, A., Nicolai, M., Okem, A., Petzold, J., Rama, B., Weyer, N.M. (Eds.), *IPCC Special Report on the Ocean and Cryosphere in a Changing Climate*. Cambridge Univ. Press, 321–445.

https://doi.org/10.1017/9781009157964.006

Pang, T., Wang, X., Nawaz, R.A., Keefe, G., Adekanmbi, T., 2023. *Coastal erosion and climate change: A review on coastal-change process processes and modeling*. Ambio 52, 2034–2052. https://doi.org/10.1007/s13280-023-01901-9

Ports and Maritime Organization (PMO), 2014. *Iran National Integrated Coastal Zone Management Plan: Process and Achievements*. Ports and Maritime Organization, Tehran, Iran.

Pourkerman, M., Marriner, N., Hamzeh, M.-A., Lahijani, H., Morhange, C., Amjadi, S., Vacchi, M., Maghsoudi, M., Shah-Hosseini, M., Afarin, M., 2022. *Socioeconomic impacts of environmental risks in the western Makran zone (Chabahar, Iran)*. Nat. Hazards 112, 1823–1849. https://doi.org/10.1007/s11069-022-05230-0

Ranasinghe, R., Ruane, A.C., Vautard, R., Arnell, N., Coppola, E., Cruz, F.A., Dessai, S., Islam, A.S., Rahimi, M., Ruiz Carrascal, D., Sillmann, J., Sylla, M.B., Tebaldi, C., Wang, W., Zaaboul, R., 2021. *Climate change information for regional impact and for risk assessment*. [In:] Masson-Delmotte, V., Zhai, P., Pirani, A., Connors, S.L., Péan, C., Berger, S., Caud, N., Chen, Y., Goldfarb, L., Gomis, M.I., Huang, M., Leitzell, K., Lonnoy, E., Matthews, J.B.R., Maycock, T.K., Waterfield, T., Yelekçi, O., Yu, R., Zhou, B. (Eds.), *Climate Change 2021: The Physical Science Basis*. Contribution of Working Group I to the Sixth Assessment Report of the Intergovernmental Panel on Climate Change. Cambridge Univ. Press, 1767–1926. https://doi.org/10.1017/9781009157896.014

Reguero, B.G., Beck, M.W., Bresch, D.N., Calil, J., Meliane, I., 2018. *Comparing the cost effectivenesscost-effectiveness of nature-based and coastal adaptation: A case study from the Gulf Coast of the United States*. PLoS One 13, e0192132. https://doi.org/10.1371/journal.pone.0192132

Reimann, L., Vafeidis, A.T., Brown, S., Hinkel, J., Tol, R.S.J., 2018. *Mediterranean UNESCO World Heritage at risk from coastal flooding and erosion due to sea-level rise*. Nat. Commun. 9, 4161. https://doi.org/10.1038/s41467-018-06645-9

Reimann, L., Vafeidis, A.T., Honsel, L.E., 2023. *Population development as a driver of coastal risk: Current trends and future pathways*. Cambridge Prisms: Coastal Futures 1, e14. https://doi.org/10.1017/cft.2023.3

Rocha, C., Antunes, C., Catita, C., 2023. *Coastal indices to assess sea-level rise impacts: A brief review of the last decade*. Ocean Coast. Manag. 237, 106536. https://doi.org/10.1016/j.ocecoaman.2023.106536

Sfreddo, G.A., da Silva, T.S., Barboza, E.G., 2023. *Assessment of local coastal vulnerability based on a global model: A case study in Jaguaruna, southern Brazil*. Reg. Stud. Mar. Sci. 61, 102824. https://doi.org/10.1016/j.rsma.2023.102824

Tahri, M., Maanan, M., Maanan, M., Bouksim, H., Hakdaoui, M., 2017. *Using Fuzzy Analytic Hierarchy Process multi-criteria and automatic computation to analyse coastal vulnerability*. Prog. Phys. Geogr. Earth Environ. 41, 268–285. https://doi.org/10.1177/0309133317695158

Thieler, E.R., Hammar-Klose, E.S., 1999. *National assessment of coastal vulnerability to sea-level rise: Preliminary results for the U.S.*, Atlantic Coast. U.S. Geological Survey Open-File Rep. 99–593. https://doi.org/10.3133/ofr99593

Tiggeloven, T., de Moel, H., Winsemius, H.C., Eilander, D., Erkens, G., Gebremedhin, E., Diaz Loaiza, A., Kuzma, S., Luo, T., Iceland, C., Bouwman, A., van Huijstee, J., Ligtvoet, W., Ward, P.J., 2020. *Global-scale benefit–cost analysis of coastal flood adaptation to different flood risk drivers using structural measures*. Nat. Hazards Earth Syst. Sci. 20, 1025–1044. https://doi.org/10.5194/nhess-20-1025-2020

Torresan, S., Furlan, E., Critto, A., Michetti, M., Marcomini, A., 2020. *Egypt's coastal vulnerability to sea-level rise and storm surge: Present and future conditions*. Integr. Environ. Assess. Manag. 16, 761–772. https://doi.org/10.1002/ieam.4280

United Nations, 1993. *Act on the Marine Areas of the Islamic Republic of Iran in the Persian Gulf and the Oman Sea*. United Nations, Division for Ocean Affairs and the Law of the Sea (DOALOS).

Vousdoukas, M.I., Mentaschi, L., Voukouvalas, E., Verlaan, M., 2017. *Extreme sea levels on the rise along Europe's coasts*. Earths Future 5, 304–323. https://doi.org/10.1002/2016EF000505

Vousdoukas, M.I., Mentaschi, L., Voukouvalas, E., Verlaan, M., Jevrejeva, S., Jackson, L.P., Feyen, L., 2018. *Global probabilistic projections of extreme sea levels show intensification of coastal flood hazard*. Nat. Commun. 9, 2360. https://doi.org/10.1038/s41467-018-04692-w

Vousdoukas, M.I., Ranasinghe, R., Mentaschi, L., Plomaritis, T.A., Athanasiou, P., Luijendijk, A., Feyen, L., 2020. *Sandy coastlines under threat of erosion*. Nat. Clim. Change 10, 260–263. https://doi.org/10.1038/s41558-020-0697-0

Ward, P.J., Jongman, B., Sperna Weiland, F.C., Bouwman, A., van Beek, L.P.H., Bierkens, M.F.P., Ligtvoet, W., Winsemius, H.C., 2013. *Assessing flood risk at the global scale: Model setup, results, and sensitivity*. Environ. Res. Lett. 8, 044019. https://doi.org/10.1088/1748-9326/8/4/044019

Zhai, L., Lee, J.-E., 2024. *Investigating vulnerability, adaptation, and resilience: A comprehensive review within the context of climate change*. Atmosphere 15, 474. https://doi.org/10.3390/atmos15040474

Zhang, Y., Ouyang, Z., Xu, C., Wu, T., Lu, F., 2024. *A multi-hazard framework for coastal vulnerability assessment*

and climate-change adaptation planning. Environ. Sustain. Indic. 21, 100327.
https://doi.org/10.1016/j.indic.2023.100327